Ultrasound in Med. & Biol., Vol. 45, No. 5, pp. 1081−1093, 2019

0301-5629/$ - see front matter

https://doi.org/10.1016/j.ultrasmedbio.2018.10.015

● *Original Contribution*

ATTENUATION COEFFICIENT ESTIMATION OF NORMAL PLACENTAS

Farah Deeba,* Manyou Ma,* Mehran Pesteie,* Jefferson Terry,† Denise Pugash,‡
Jennifer A. Hutcheon,§ Chantal Mayer,§ Septimiu Salcudean,* and Robert Rohling*,¶

* Department of Electrical and Computer Engineering, University of British Columbia, Vancouver, British Columbia, Canada; † Department of Pathology and Laboratory Medicine, University of British Columbia, Vancouver, British Columbia, Canada; ‡ Department of Radiology, University of British Columbia, Vancouver, British Columbia, Canada; § Department of Obstetrics and Gynaecology, University of British Columbia, Vancouver, British Columbia, Canada; and ¶ Department of Mechanical Engineering, University of British Columbia, Vancouver, British Columbia, Canada

(*Received* 23 *June* 2018; *revised* 18 *September* 2018; *in final from* 10 *October* 2018)

Abstract—Attenuation coefficient estimation has the potential to be a useful tool for placental tissue characterization. A current challenge is the presence of inhomogeneities in biological tissue that result in a large variance in the attenuation coefficient estimate (*ACE*), restricting its clinical utility. In this work, we propose a new Attenuation Estimation Region Of Interest (AEROI) selection method for computing the *ACE* based on the (i) envelope signal-to-noise ratio deviation and (ii) coefficient of variation of the transmit pulse bandwidth. The method was first validated on a tissue-mimicking phantom, for which an 18%−21% reduction in the standard deviation of *ACE* and a 14%−24% reduction in the *ACE* error, expressed as a percentage of reported *ACE*, were obtained. A study on 59 post-delivery clinically normal placentas was then performed. The proposed AEROI selection method reduced the intra-subject standard deviation of *ACE* from 0.72 to 0.39 dB/cm/MHz. The measured *ACE* of 59 placentas was 0.77 ± 0.37 dB/cm/MHz, which establishes a baseline for future studies on placental tissue characterization. (E-mail: farahdeeba@ece.ubc.ca) **© 2018 World Federation for Ultrasound in Medicine & Biology. All rights reserved.**

Key Words: **Attenuation coefficient estimate, Placenta, Envelope signal-to-noise ratio, Pulse bandwidth, Reference phantom method.**

INTRODUCTION

The accurate and objective estimation of the amplitude attenuation coefficient has important clinical implications. The accuracy of attenuation coefficient estimation strongly influences the measurement accuracy of the other quantitative ultrasound parameters including backscatter coefficient, effective scatterer diameter and spacing (Oelze and O'Brien 2002). In addition, the attenuation coefficient estimate (*ACE*) has independently been used in the detection of different pathologic states. The majority of clinical studies on *ACE* have been performed on diffuse liver disease. Researchers found a positive correlation between fat infiltration in liver and *ACE* (Lu et al. 1999; Kanayama et al. 2013). Other studies have reported that thefrequency dependence of attenuation has diagnostic and prognostic value in characterizing breast tissue (D'Astous and Foster 1986; Nam et al. 2013), myocardial tissue (O'Donnell et al. 1981), carotid artery plaques (Shi et al. 2009) and osteoporosis (Glüer 1997; Wear 2003).

In the field of obstetrics, the utility of *ACE* is being explored to predict pregnancy-related complications. Attenuation change in the cervix has been found to be correlated with cervical ripening, an early indicator of labor onset (Yassin et al. 2011). Other *in vivo* studies have found that the cervical attenuation coefficient is positively correlated to the interval between the ultrasound examination and delivery. However, *in vivo ACE* has not been found to be correlated to gestational age or cervical length (Bigelow et al. 2008; McFarlin et al. 2010). In the early 1980s, researchers started exploring the use of *ACE* in the placenta alongside fetal liver and fetal lung, with the aim of assessing fetal maturity and diagnosing intrauterine growth restriction (Flax et al. 1983). Benson et al. (1983) hypothesized that attenuation and scattering properties of placental tissue may change

Address correspondence to: Farah Deeba, Department of Electrical and Computer Engineering, University of British Columbia, 2332 Main Mall, Vancouver, BC V6T 1Z4, Canada. E-mail: farahdeeba@ece.ubc.ca

with maturation as a result of an increase in collagen content and fibrin deposition. They reported a relative increase in the slope of the frequency-dependent attenuation coefficient with the maturation of placental tissue ($n = 16$). A more recent *ex vivo* study found a positive correlation of gestation age with the placental attenuation coefficient ($n = 12$) (Caloone et al. 2015). None of the studies to date are sufficiently large to form a statistical baseline for the normal placental attenuation coefficient. A larger cohort study establishing baseline attenuation levels is needed as the first step for reliable comparison studies between normal and diseased placentas.

The *ACE* is specified in decibels of ultrasound amplitude dissipated per centimeter of propagation per megahertz because of a combined effect of scattering and absorption. An ultrasound pulse is attenuated as an exponential function of depth penetrated with a power law dependence (where the power law exponent ranges between 0.8 and 1.2 for biological tissue) in the frequency range of a typical ultrasound scanner. Therefore, spectral methods measure the *ACE* based on the change in spectral contents, that is, amplitude decay or center frequency downshift in the backscattered power spectrum along the depth (Hyungsuk and Varghese 2007; Labyed and Bigelow 2011). However, there are additional mechanisms such as diffraction and backscatter variation that also affect the spectrum of the backscattered radio frequency (RF) signal. The spectral difference method, also referred to as the reference phantom method, compensates for diffraction and other system-dependent effects by utilizing a well-characterized reference phantom (Yao et al. 1990). However, the reference phantom method does not compensate for the backscatter variation within the region of interest (ROI), which may both be depth and frequency dependent. A change in frequency dependence of backscatter along the penetration depth would result in variation in the bandwidth of the backscattered spectrum, which is unrelated to the attenuation variation (Flax et al. 1983). Therefore, the reference phantom method will be erroneous when the tissue ROI under consideration is not homogeneous. The selection of suitable ROIs is therefore needed to ensure accurate measurement of *ACE*.

The placenta undergoes a gradual change in ultrasonic appearance during its maturation process. An immature placenta is homogeneous, whereas a mature placenta is irregular with prominent undulations (*i.e.,* indentations) and scattered echogenic areas (Grannum et al. 1979). The inhomogeneity of matured placentas poses a challenge in selecting suitable attenuation estimation regions (AERs) required for low-variance and accurate computation of *ACE*. In addition, the attenuation estimation methods, which are typically validated on simulation data and well-characterized reference phantoms, may yield unreliable *ACE* measures in clinical applications because of several factors. Among these factors, envelope signal-to-noise ratio (SNR) and sound speed mismatch (Omari et al. 2011; Rubert and Varghese 2014); difference in scatterer size and distribution between the reference phantom and the tissue under investigation (Omari et al. 2013; Rubert and Varghese 2014) and within the tissue region-of-interest (Labyed and Bigelow 2011); and violation of stationary and incoherent scattering condition in tissue (Rosado-Mendez et al. 2016) are a few of them. Therefore, large estimation variance including infeasible negative attenuation coefficients may result (Bigelow et al. 2008; Rubert and Varghese 2014).

The objective of the study described here was to establish an *ACE* measurement method with lower variance and higher accuracy suitable for *ex vivo* placentas. To this end, we define a new attenuation estimation region of interest (AEROI) selection method to ensure homogeneity and consistency in backscatter frequency dependence, two key assumptions for the reference phantom method. Additionally, we analyze the effect of AEROI parameters and optimize the parameter values to achieve minimum estimate variance. We analyze the variation in *ACE* obtained from tissues near the fetal surface compared with the maternal surface. Finally, we report the *ACE* values measured from the selected AEROIs using the reference phantom method for clinically normal placentas.

THEORY

Reference phantom method

First, we briefly review the reference phantom method, which has been used primarily for *ACE* computation in this work. The reference phantom method accounts for system-dependent parameters and requires smaller regions to compute *ACE* compared with other methods (Rosado-Mendez et al. 2013). In the reference phantom method (Yao et al. 1990), the RF data are acquired from both the tissue sample under experiment and a well-characterized reference phantom using the same transducer and system settings. For a time-gated RF signal window centered at depth z, the ratio of the power spectrum S from the sample to the reference phantom at frequency f can be written as (Labyed and Bigelow 2011; Nam et al. 2011):

$$RS(f,z) = \frac{S_s(f,z)}{S_r(f,z)} = \frac{G_s(f)D_s(f,z)A_s(f,z_0)B_s(f,z)e^{-4\alpha_s(f)(z-z_0)}}{G_r(f)D_r(f,z)A_r(f,z_0)B_r(f,z)e^{-4\alpha_r(f)(z-z_0)}}. \quad (1)$$

Here, the "s" and "r" subscripts denote sample and reference, respectively, $G(f)$ represents the transducer transfer function and transmit pulse, $D(f;\ z)$ denotes the diffraction effects related to transducer geometry and beamforming, $A(f;\ z_0)$ is the total attenuation effect from the transducer surface to the depth z_0, which corresponds to the beginning of the ROI, $B(f;\ z)$ represents the backscatter coefficient of the medium within the ROI, α is the attenuation coefficient within the ROI and z is the distance from the transducer surface to the center of a particular time-gated RF signal window within the ROI.

Using the same system settings and assuming the same sound speed in the tissue sample and reference phantom allow us to cancel the system-dependent terms, namely, $G(f)$ and $D(f;\ z)$. Additionally, the assumption of homogeneity within the ROI ensures that the backscatter coefficient, $B(f;\ z) = B(f)$ remains constant along penetration depth inside the ROI. Therefore, eqn (1), after taking the natural logarithm, reduces to

$$ln[RS(f,z)] = 4(\alpha_r(f) - \alpha_s(f))(z - z_0) + ln\left[\frac{A_s(f,z_0)B_s(f)}{A_r(f,z_0)B_r(f)}\right]. \quad (2)$$

The attenuation of the sample at each frequency component, $\alpha_s(f)$ (Np/cm), can be calculated from the slope of the straight line that fits eqn (2), that is,

$$\alpha_s(f) = \alpha_r(f) - \frac{1}{4}\frac{\partial[\ln(RS(f,z))]}{\partial(z)}. \quad (3)$$

We assume a linear frequency dependence of attenuation, α_s (Np/cm), within the usable bandwidth of the ultrasound transducer, which is a good approximation for several soft tissues including placental tissue (Caloone et al. 2015). Therefore, the *ACE*, denoted by β_s (Np/cm/MHz), can be determined by finding the slope of the straight line that fits the equation

$$\alpha_s(f) = \beta_s f. \quad (4)$$

The reference phantom method is based on several simplifying assumptions. A critical assumption for the reference phantom method is homogeneity within the ROI with the same scatterer density and same scatterer size (*i.e.,* invariant frequency dependence of backscatter). Violation of the homogeneity assumptions leads to inaccurate estimate of the *ACE* (Labyed and Bigelow 2011). Therefore, it is necessary to ensure the selection of a ROI where the assumptions of the reference phantom methods are met.

AEROI selection parameters

The placental region imaged in a scan includes multiple possible AERs, allowing the selection of a set of AERs that satisfy conditions for accurate *ACE* measurement. AER is defined as the region from which a single *ACE* is obtained, whereas AEROI is the aggregate of AERs selected based on a set of proposed parameters. The proposed parameters, envelope SNR deviation (ΔSNR_e) and coefficient of variation of the transmit pulse bandwidth (CoV_{FWHM}), are intended to ensure the identification of a region where crucial assumptions of the reference phantom methods are satisfied.

Envelope SNR deviation. Envelope SNR (SNR_e), defined as the ratio of the mean to the standard deviation of the RF signal envelope, can serve as a metric of homogeneous texture. A previous study reported that as the SNR_e approaches 1.91, the SNR of the Rayleigh distribution, the *ACE* in the reference phantom method is more precise (Rubert and Varghese 2014). This is because spectral methods are based on the underlying assumption that RF signal generation is a stationary scattering process, arising from a large number of randomly distributed scatterers identical in size (Shankar et al. 1996). This is called fully developed speckle and leads to the Rayleigh distribution for the RF signal envelope. The Rayleigh distribution implies homogeneity of the medium, which is an important assumption for the reference phantom method. Therefore, we choose envelope SNR deviation, ΔSNR_e, as an AEROI selection parameter, which is defined as

$$\Delta SNR_e = \frac{\left|SNR_e - SNR_{opt}\right|}{SNR_{opt}} \times\ 100\%, \quad (5)$$

where $SNR_{opt} = 1.91$, which is the average SNR of Rayleigh distribution. SNR_e is the envelope SNR of the sample under investigation. The envelope SNR is defined as

$$SNR_e = \frac{\langle \mathrm{E} \rangle}{\sqrt{\langle (\mathrm{E} - \langle \mathrm{E} \rangle)^2 \rangle}}, \quad (6)$$

where $\langle\rangle$ denotes expectation, and E are the RF signal envelope values over the AERs.

CoV of transmit pulse bandwidth. We assume that the backscatter coefficient $B(f)$ is depth invariant, which allows us to derive the attenuation estimation equation (eqn [3]). $B(f)$ can be modeled as a power function of frequency and can be approximated by an exponential form of the lower-order terms in a Taylor series expansion. For an ultrasound transmit pulse with a Gaussian-shaped envelope, center frequency f_c and variance σ^2,

$$B(f) = f^n \propto exp\left[-\frac{n.(f^2 - 4f_c f)}{2f_c^2}\right], \quad (7)$$

where n is the characteristic scatter exponent, which varies from 0 for a specular reflection to 4 for pure Rayleigh scatterers (Flax et al. 1983). If n changes abruptly within the AER, the term $B(f; z)$ remains depth dependent and eqn (2) will not hold.

The violation of the assumption is reflected as a change in the Gaussian characteristics of the ultrasound pulse. The amount of centroid shift and the bandwidth are both modified by the frequency-dependent backscatter process, whereas the bandwidth remains unaltered in the presence of attenuation process alone (Flax et al. 1983; Kuc et al. 1976). The variation of the characteristic scatter exponent n modifies the ultrasound pulse bandwidth according to the equation:

$$\hat{\sigma}^2 = \sigma^2 \frac{f_c^2}{f_c^2 + n\sigma^2}. \tag{8}$$

We can quantify the variation of n with depth by computing the variation in ultrasound pulse bandwidth. Given that pulse variance at depth z_1 is σ_1^2, and that at depth z_2 is σ_2^2, eqn (8) would lead to the relationship

$$\sigma_1^2 - \sigma_2^2 \propto n_1 - n_2. \tag{9}$$

We propose to measure the variation in pulse bandwidth by computing the CoV of the pulse spectrum's full width at half-maximum (FWHM). CoV gives the measure of dispersion of bandwidth from the mean value along the propagation depth. The CoV of the transmit pulse bandwidth is defined as

$$CoV_{\mathrm{FWHM}} = \frac{\mathrm{SD(FWHM)}}{\mu(\mathrm{FWHM})} \times \ 100\% \tag{10}$$

where SD is the standard deviation, and μ is the mean of the FWHM values of ultrasound power spectra along the depth.

The above-described AEROI selection parameters are utilized to find an optimum AEROI, where RF data follow the assumptions required for the reference phantom method.

METHODS

Scanning system overview and data acquisition

The ultrasound RF data from the reference phantom and *ex vivo* placentas were acquired with an Ultrasonix SonixTouch ultrasound machine (Analogic, Richmond, BC, Canada) using a 4DL14-5/38 4D linear transducer operated at 5-MHz center transmit frequency. The time-gain compensation, power level, depth and focus were adjusted to ensure optimum image quality for placenta samples. Accordingly, the depth was set to 3 cm with a focus at 2 cm to capture the full thickness of the full-term placentas. The system was equipped with the Porta research interface, which enables development of a software module (SWAVE system), designed primarily as an elastography system (Abeysekera 2016; Abeysekera et al. 2017). The system collects volumetric RF data by sweeping a 2-D frame over 10 elevation angles, with an angle increment of 0.4°. Each 2-D frame in the 3-D volume consists of 128 RF scanlines spaced at 0.295 mm. The sampling rate was 40 MHz, resulting in 1568 samples in each scanline.

Tissue-mimicking phantoms

Before its application to the placenta data, the effectiveness of the AEROI selection method was validated on a tissue-mimicking phantom. The RF data acquired from the phantom were also used as the reference for the reference phantom method. The multi-purpose multi-tissue ultrasound phantom (Model 040GSE) manufactured by CIRS (Norfolk, VA, USA) was made of proprietary Zerdine hydrogel polymer. The phantom has two separated attenuation regions with attenuation coefficients of 0.7 (±0.07) and 0.95 (±0.07) dB/cm/MHz and a speed of sound of 1540 m/s as reported by the manufacturer. It contains nylon monofilaments as scattering targets of different size and therefore different frequency dependence compared with that of the background. The phantom also includes targets made of same material as the background with different scatterer density.

Study population

Placentas (gestational age between 37 and 41 wk) were collected after delivery from pregnant women between the ages of 19 and 47 y ($n = 59$). This study (H15-00974) was performed under written informed consent after approval by the University of British Columbia Children's and Women's Research Ethics Board. After delivery, the placentas were immediately stored at 4°*C* for an average of 4 h and warmed to 37°C by submersion in a constant-temperature water bath (Cole-Parmer, Montreal, QC, Canada) to simulate the *in vivo* temperature before acquiring RF data (Abeysekera et al. 2017). In this study, women with an uncomplicated term pregnancy were recruited based on the clinical presentation. After delivery, all placentas underwent pathologic examination performed by a placental pathologist. After examination, the placentas in this study were subdivided into three categories (Table 1) (Khong et al. 2016). Category A included 13 placentas without any specific lesions, category B included 30 placentas manifesting specific lesions that did not reach a diagnostic threshold and category C comprised the remaining 16 placentas with abnormalities passing one or more diagnostic thresholds. It should be emphasized that regardless of the presence of the lesions, all the

Table 1. Description of sub-categories in *ex vivo* placenta dataset.

Sub-Category	Description	Sample Size
A	No appreciable abnormalities	13
B	Abnormalities that are within a diagnostic threshold	30
C	Abnormalities passing one or more diagnostic thresholds	16

placentas were considered to be clinically normal based on the criteria that the pregnancies had no clinical complications. Therefore, the categories include subclinical pathologic changes that may be found in clinically normal placentas, recognizing that it is normal for all placentas to accrue some abnormalities over time. These abnormalities may produce areas of inhomogeneity.

RF data processing and analysis

The attenuation coefficient estimation algorithm was implemented in MATLAB 2016a (The MathWorks Inc., Natick, MA, USA). For the tissue-mimicking reference phantom, a ROI was defined axially from 6 to 30 mm to exclude the near-field data suffering from ringdown and other artifacts associated with transducer-to-phantom surface (Nam et al. 2011). For the placenta samples, the ROI was defined as the maximum rectangular area containing only placenta tissue.

The RF data within the selected ROIs were divided into overlapping AERs. The consecutive AERs were spaced at one axial correlation length apart and one lateral correlation length apart in the axial and lateral directions, respectively. Correlation length was defined as the range of spatial lags (number of samples axially, and scanlines laterally) over which the one-sided correlation coefficient remained >2% (Rosado-Mendez et al. 2013). The spacing allowed uncorrelated estimates of the parameters (Rosado-Mendez et al. 2016).

Each AER was divided into a number of time-gated windows spaced one axial correlation length apart (Rosado-Mendez et al. 2013). Initially, the dimensions for the time-gated windows were selected to be N = 30 scanlines (8 uncorrelated scanlines) laterally and $\Delta z = 7.7$ mm (400 samples or ~24 pulse lengths) axially. We investigated the effect of time-gated window parameters on *ACE* variance and error by varying N from 1 to 50 and Δz from 20 to 130 mm. We kept the number of time-gated windows in each AER fixed at 5.

The Welch method (Welch 1967) was used to obtain the power spectrum from the RF scanlines within each time-gated window across the 10 acquired planes. According to the Welch method, each RF scanline within a time-gated window was subdivided into overlapping sections, with length equal to 50% of the original RF scanline and with 50% overlap (50% overlap minimizes the power spectral density estimation variation [Welch 1967]). Each segment was then multiplied with a Hamming window. The power spectral density was obtained after averaging the periodograms obtained from the windowed segments. We considered the −10 dB bandwidth of the received power spectrum as the usable frequency range. The power spectral density values obtained at the time-gated windows of each AER were used as the regression points to compute the rate of amplitude decay along the propagation depth. The slope estimates obtained from the regression analysis were used to compute *ACE*. The AEROI selection parameters ΔSNR_e and CoV_{FWHM} were computed at each time-gated window and averaged over the windows in an AER to obtain a single value for each parameter corresponding to each AER. The AERs where ΔSNR_e and CoV_{FWHM} values satisfied the empirically determined thresholding criteria were selected for subsequent processing. An AEROI was defined to be the aggregate of the selected AERs.

The non-parametric Mann−Whitney *U*-test and the Kruskal−Wallis test were used to compare the statistical significance of the difference between mean *ACE* and standard deviation of *ACE* of placentas computed with and without AEROI selection criteria, among *ACE*s of placentas from different categories and among *ACE*s of tissue near fetal and maternal surfaces of placentas. We consider a p value < 0.05 as indicating statistical significance.

AEROI selection method

Based on the AEROI selection parameters, we define an AEROI selection method in this section. First, we examine the effect of AEROI selection parameters on attenuation estimation accuracy. We manually select two different regions in the tissue-mimicking phantom from the 0.95 dB/cm/MHz layer and one from the 0.7 dB/cm/MHz attenuation layer, representing three different cases. Case I represents a homogeneous region (0.95 dB/cm/MHz), case II includes nylon scattering targets representing an inhomogeneous region with varying frequency dependence of backscatter (0.95 dB/cm/MHz) and case III represents an inhomogeneous region including variation in scatterer density (0.7 dB/cm/MHz).

Figure 1 illustrates the correlation between the AEROI selection parameter values and *ACE* error. In the homogeneous region (case I), CoV_{FWHM} and ΔSNR_e both remain below 10%. The *ACE* error in the homogeneous region also remains below 0.19 dB/cm/MHz (20% of the actual value). Case II includes two targets causing variation in the frequency dependence of backscatter. We can recognize two peaks in the *ACE* error corresponding to two peaks in ΔSNR_e deviation curve representing 37% and 30% deviation. There was also a

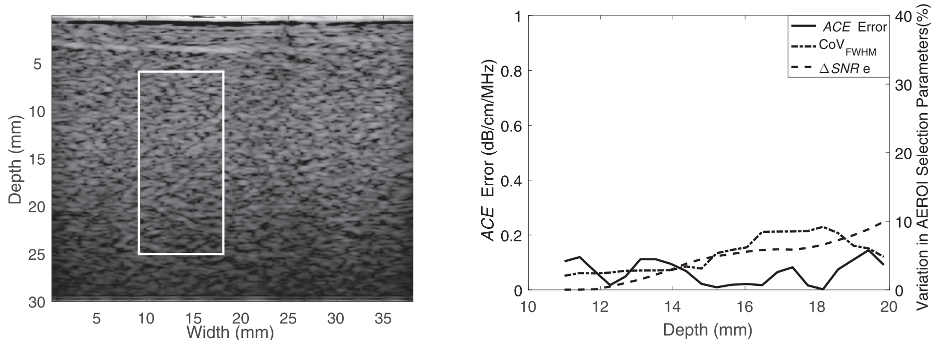

(a) case I

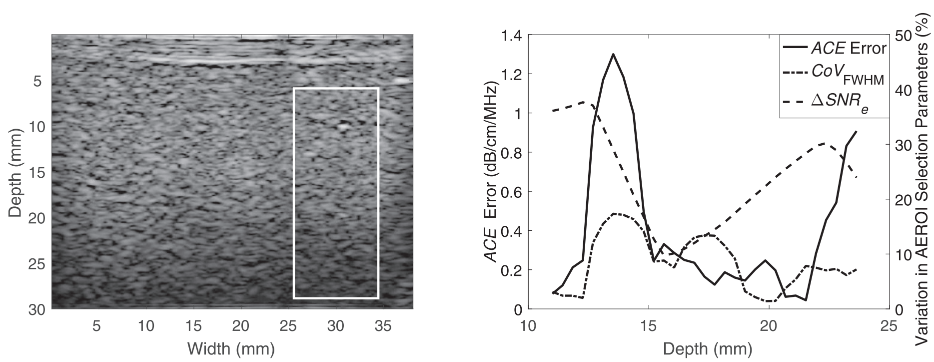

(b) case II

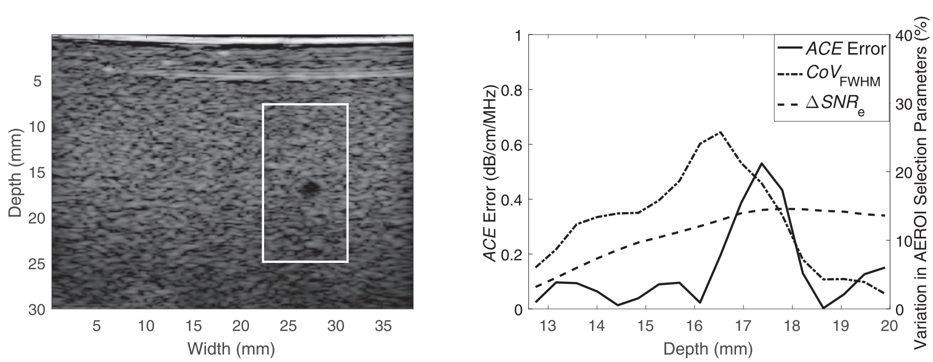

(c) case III

Fig. 1. Effect of AEROI selection parameters on *ACE* error. Left: B-Mode images with manually selected regions of interest representing three different cases for the 0.95 dB/cm/MHz attenuation layer (cases I and II) and 0.7 dB/cm/MHz attenuation layer (case III) of a tissue-mimicking phantom. Right: Variation in AEROI selection parameters ΔSNR_{e} and CoV_{FWHM}, and corresponding error in *ACE* along the depth of regions of interest. *ACE* = attenuation coefficient estimate; AEROI = attenuation estimation region of interest; ΔSNR_{e} = envelope SNR deviation; SNR = signal-to-noise ratio; CoV_{FWHM} = CoV of transmit pulse bandwidth; CoV = coefficient of variation.

moderate increase in CoV_{FWHM} (17%). For case III corresponding to an inhomogeneous region with varying scatterer density, the spike representing an *ACE* error of 106% corresponds to increases in CoV_{FWHM} (by 26%) and ΔSNR_{e} (17%). We also noticed that there was a spatial lag between the pattern in the ΔSNR_{e} and *ACE* error. This can be explained by the limited spatial resolution and complex spatial dependence of the backscatter process. However, appropriate thresholding will enable selection of AERs from homogeneous regions. We empirically set a threshold for CoV_{FWHM}, $T_{CoV(\mathrm{FWHM})}$ and a threshold for ΔSNR_{e}, $T_{\Delta SNR\mathrm{e}}$ and define the criteria for selecting homogeneous AERs as follows:

$$EAR(\Delta SNR_e, \mathrm{CoV}_{\mathrm{FWHM}}) = \begin{cases} \text{"homogeneous", if } \Delta SNR_e < T_{\Delta SNR_e} \\ \quad \text{and } CoV_{\mathrm{FWHM}} < T_{CoV(\mathrm{FWHM})}; \\ \quad \text{"inhomogenous", otherwise.} \end{cases}$$

The threshold $T = \left[T_{\Delta SNR_e},\ T_{CoV(\mathrm{FWHM})}\right]$ for each ROI is empirically defined as

$$T = \left[\min\left(T_{\Delta SNR_e}\right), \min\left(T_{CoV(\mathrm{FWHM})}\right)\right] \text{ such that } N_{\mathrm{AER}} > N_{\min}, \tag{11}$$

where N_{AER} is the number of selected AERs and $N_{\min}$ is a constant. $N_{\min}$ was defined as a fraction of the total number of AERs for each subject. We empirically select a $N_{\min}$ value that gives a reasonable estimate variance for all the patients.

EXPERIMENTAL RESULTS

Time-gated window dimension

We experimented with different window sizes, varying numbers of scanlines N from 1 to 50 and window lengths Δz from 19.13 mm (100 samples or ≈ 6 pulse length) to 134 mm (700 samples or ≈ 41 pulse length) for tissue-mimicking reference phantoms. The results for both the 0.95 and 0.7 dB/cm/MHz layers are illustrated in Figure 2. We found the minimum window dimension to be $\Delta z = 5$ mm (260 samples or ≈ 15 pulse length) and $N = 25$ lateral scanlines from 10 parallel planes (6 uncorrelated scanlines × 10 = 60) for a stable and accurate ACE measurement.

Validation of AEROI selection method on tissue-mimicking phantom

The proposed AEROI selection method lower-bounds the threshold by the constraint of ensuring a sufficient number of AERs. We require a sufficient number of AERs to reduce spatial variance noise. To fully appreciate the effect of the AEROI selection method on the accuracy and variance of ACE with respect to the number of selected AERs, we plotted mean ACE error, standard deviation of ACE and fractional AER count as functions of $T_{\Delta SNR_e}$ and $T_{CoV(\mathrm{FWHM})}$. Figure 3 provides an example of a tissue-mimicking phantom (0.95 dB/cm/MHz layer) for which the attenuation error and standard deviation monotonically increase with the threshold values. This means we can improve the ACE accuracy and reduce the variance by more than 50% while retaining 60% of the total AERs. Though these statistics are highly dependent on the homogeneity of a particular

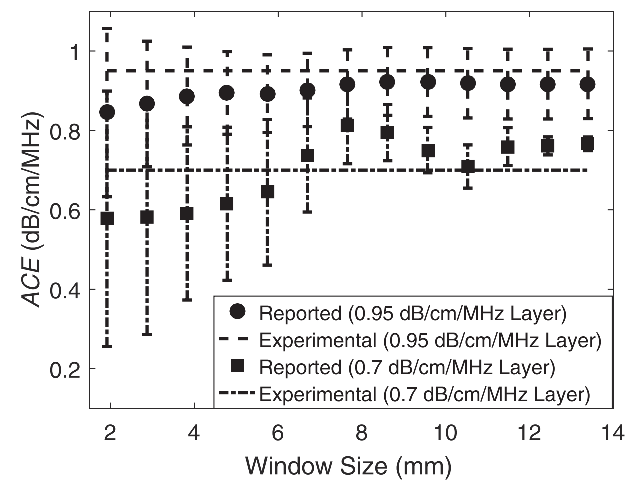

(a)

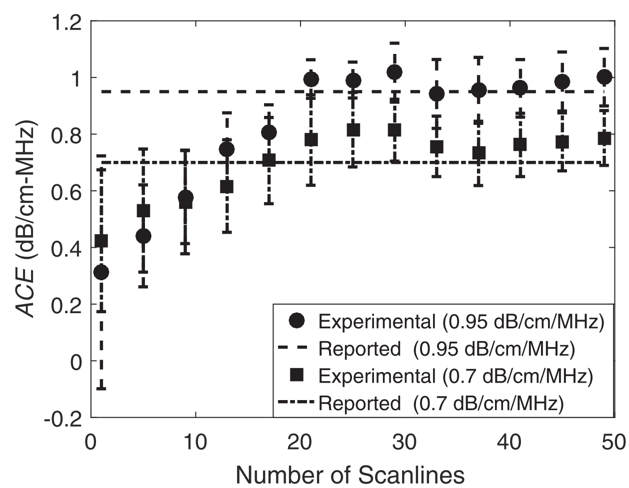

(b)

Fig. 2. Effect of time-gated window dimension on attenuation coefficient estimate variance and accuracy. (a) Attenuation coefficient estimate obtained using different window lengths; (b) Attenuation coefficient estimate obtained with different numbers of radio frequency scanlines taken from each of the 10 parallel planes. The dashed error bars and the dash-dotted error bars represent the standard deviations of estimated values for the 0.95 and 0.7 dB/cm/MHz attenuation layers, respectively. ACE = attenuation coefficient estimate.

sample, it justifies the importance of AEROI selection criteria for improving ACE accuracy and precision.

We report the average envelope SNR deviation (ΔSNR_e) and CoV of pulse full width at half-maximum (CoV_{FWHM}) values for the tissue-mimicking phantom in Table 2. We also report the ACE values obtained before and after applying the AEROI selection criteria. For homogeneous regions, all AERs are homogeneous, and therefore, the mean and standard deviation of ACE remain unaffected after applying AEROI selection

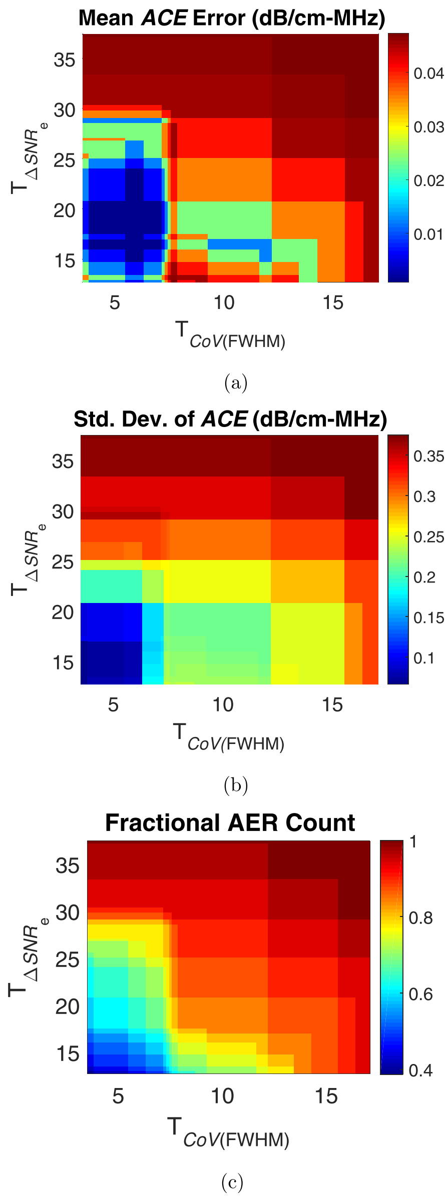

Fig. 3. Effect of threshold, *T,* on attenuation coefficient estimate. Color plots reveal (a) correlation between *ACE* error and threshold values; (b) correlation between standard deviation of *ACE* and threshold values; and (c) correlation between number of AERs selected as a fraction of the total number of AERs and threshold values. *ACE* = attenuation coefficient estimate; AER = attenuation estimation region; CoV = coefficient of variation; SNR = signal-to-noise ratio.

criteria. For case II, applying AEROI selection criteria reduces the *ACE* error from 30% to 6% and the standard deviation from 54% to 36%, expressed as the percentage of the reported *ACE* value. For case III, the *ACE* error is reduced from 15% to 0.8% of the reported *ACE*. It also reduces the standard deviation from 40% to 19% of the reported *ACE*. The effect of AEROI selection criteria is more prominent for case II, which corresponds to scatterers of different size (*i.e.,* varying frequency dependence of backscatter). The results from case II emphasize that the variation in backscatter frequency dependence has a comparatively severe effect on *ACE*, which is in agreement with the previous literature (Labyed and Bigelow 2011).

Attenuation coefficient estimates for ex vivo *placenta data*

We estimated the mean and standard deviation of the AEROI selection parameter values for placenta samples. The results are listed in Table 3. The envelope SNR values obtained were lower than SNR_{opt} and SNR_{e} for the phantom, whereas CoV_{FWHM} values were found to be in a range similar to that in the phantom.

Figure 4 illustrates the effect of applying AER selection criteria to an example placenta sample. The sample has appreciable inhomogeneity within the selected ROI. Evaluating *ACE* for all the AERs in the ROI results in a large estimate variance. From the attenuation map, we find that the outlying estimate values are caused predominantly by the inhomogeneities. The regions with outlying *ACE* values overlap with high AEROI selection parameter values in the ΔSNR_{e} map or CoV_{FWHM} map. Therefore, the AEROI selection criteria successfully remove the outlier values, retaining 20 out of total of 228 AERs and resulting in an *ACE* with lower variance.

We report the mean *ACE* values and the intra-subject standard deviations of *ACE* values obtained for the placentas in each category and also for all placental data in Table 3 before and after applying the AEROI selection method. To select the threshold *T*, the minimum number of AERs, $N_{\min}$, was set at 10% of the total number of AERs. The averages of the mean *ACE*s were 0.82 and 0.77 dB/cm/MHz before and after applying AEROI

Table 2. AEROI selection parameter values and *ACE* for tissue-mimicking phantom

Reported *ACE* (dB/cm/MHz)	ΔSNR_{e} (%)	CoV_{FWHM} (%)	*ACE* (dB/cm/MHz)	ACE_{AEROI} (dB/cm/MHz)
Case I: 0.95	4.39 ± 2.98	5.16 ± 2.54	0.943 ± 0.107	0.945 ± 0.130
Case II: 0.95	23.61 ± 8.79	8.38 ± 5.01	1.235 ± 0.509	1.001 ± 0.34
Case III: 0.7	9.23 ± 4.37	11.14 ± 4.0	0.805 ± 0.276	0.706 ± 0.133

ACE = attenuation coefficient estimate; AEROI = attenuation estimation region of interest; CoV_{FWHM} = CoV of transmit pulse bandwidth; CoV = coefficient of variation; ΔSNR_{e} = envelope SNR deviation; SNR = signal-to-noise ratio.

Table 3. AEROI selection parameter values and ACE results for *ex vivo* placenta

Category	ΔSNR_e(%)	CoV_{FWHM}(%)	*ACE* (dB/cm/MHz)	ACE_{AEROI} (dB/cm/MHz)
A	42.44 ± 18.73	4.88 ± 4.96	0.82 ± 0.64	0.73 ± 0.38
B	46.73 ± 17.60	6.37 ± 8.25	0.85 ± 0.75	0.76 ± 0.39
C	43.48 ± 16.46	6.27 ± 7.13	0.80 ± 0.69	0.94 ± 0.43
Total	44.84 ± 17.67	5.99 ± 7.32	0.82 ± 0.72	0.77 ± 0.39

ACE = attenuation coefficient estimate; AEROI = attenuation estimation region of interest; CoV_{FWHM} = CoV of Transmit Pulse bandwidth; CoV = coefficient of variation; ΔSNR_e = envelope SNR deviation; SNR = signal-to-noise ratio.

selection, respectively. The mean *ACE* values before and after applying AEROI selection were not significantly different ($p = 0.81$). The standard deviation of *ACE* within each subject was 0.39 dB/cm/MHz after AEROI selection, which was significantly lower than that (0.72 dB/cm/MHz) obtained before AEROI selection ($p = 7.81 \times 10^{-8}$). The distribution of intra-subject mean and standard deviation is illustrated in Figure 5.

The inter-subject standard deviation for the three categories of placenta classification were 0.28, 0.39 and 0.55 dB/cm/MHz, respectively, and the overall inter-subject standard deviation was 0.37 dB/cm/MHz. In Figure 6 are the box-and-whisker representations of ACE_{AEROI} for three categories of the placenta. The differences among the three categories do not reach statistical significance ($p = 0.71$) according to the Kruskal−Wallis test. The result agrees with previous work based on the same data set in which no significant difference was found for shear wave speed among these three categories (Abeysekera et al. 2017). In other words, the presence of placental abnormalities in clinically normal patients did not significantly affect *ACE*s.

In addition, we compared the ACE_{AEROI} values from regions near the maternal surface and the fetal surface obtained before and after thresholding. The box-and-whisker plot is provided in Figure 7. We found that the fetal side is associated with slightly higher attenuation coefficients compared with the maternal side ($p = 9.34 \times 10^{-16}$).

DISCUSSION

Only a few studies reporting the *ACE*s for placenta are available. Given the absolute value of the *ACE*, the values measured in this study can be directly compared with those from existing studies. Using the proposed reference phantom method, we obtained an average *ACE* of 0.77 ± 0.37 dB/cm/MHz for *ex vivo* placentas at 37−41 wk ($n = 59$). Akaiwa (1989) reported an *ACE* of 0.4 ± 0.11 dB/cm/MHz for *in vivo* normal placentas at 34 wk of gestational age ($n = 13$). Caloone et al. (2015) reported an *ACE* of 0.76−0.85 dB/cm/MHz for *ex vivo* placenta at 36−40 wk ($n = 4$). Moreover, the study was designed to apply high-intensity focused ultrasound to create placental lesions, and therefore, the clinical conditions were not among the selection criteria. Our study is the largest study to date to report *ACE*s of normal *ex vivo* placentas.

We analyzed the effect of the time-gated window dimension of *ACE*. Rosado-Mendez et al. (2013) have emphasized the importance of uncorrelated samples in reducing coherent noise components in power spectral density estimates. The minimum required window length in our study is 15 pulse lengths, which is in the range of widely accepted window length (7−15 pulse lengths) (Liu et al. 2010; Rosado-Mendez et al. 2013). However, the number of minimum independent scanlines is found to be equal to 60 (6 uncorrelated scanlines from 10 parallel planes), which is higher ($N = 60$) than the range of 10−20 independent scanlines suggested in different studies (Liu et al. 2010; Rosado-Mendez et al. 2013). A possible reason for the bias could be that the consecutive parallel acquisitions of ultrasound planes are not completely uncorrelated.

In this article, we have discussed the importance of homogeneity criteria, a fundamental assumption for the reference phantom method for accurate and precise estimation of *ACE*. We have proposed a new AEROI selection method to ensure the selection of a region that satisfies the underlying assumptions for the reference phantom method. We found that changes in scatterer density and scatterer size influence the envelope SNR and the pulse bandwidth. Defining AEROI selection criteria based on thresholding of the parameters, namely, envelope SNR deviation and CoV of pulse FWHM, allows homogeneous regions to be optimally chosen. The proposed method improves the estimate variance significantly, reducing the intra-subject standard deviation from 0.72 to 0.39 dB/cm/MHz.

Several works have acknowledged the difficulty in achieving *ACE*s with low variance. It has been found that biological variation is a minor contributing factor (Bigelow et al. 2008), whereas a large deviation in envelope SNR from 1.91 is responsible for high estimate variance (Rubert and Varghese 2014). In addition, Kuc et al. (1976) reported that ultrasound pulse shape and

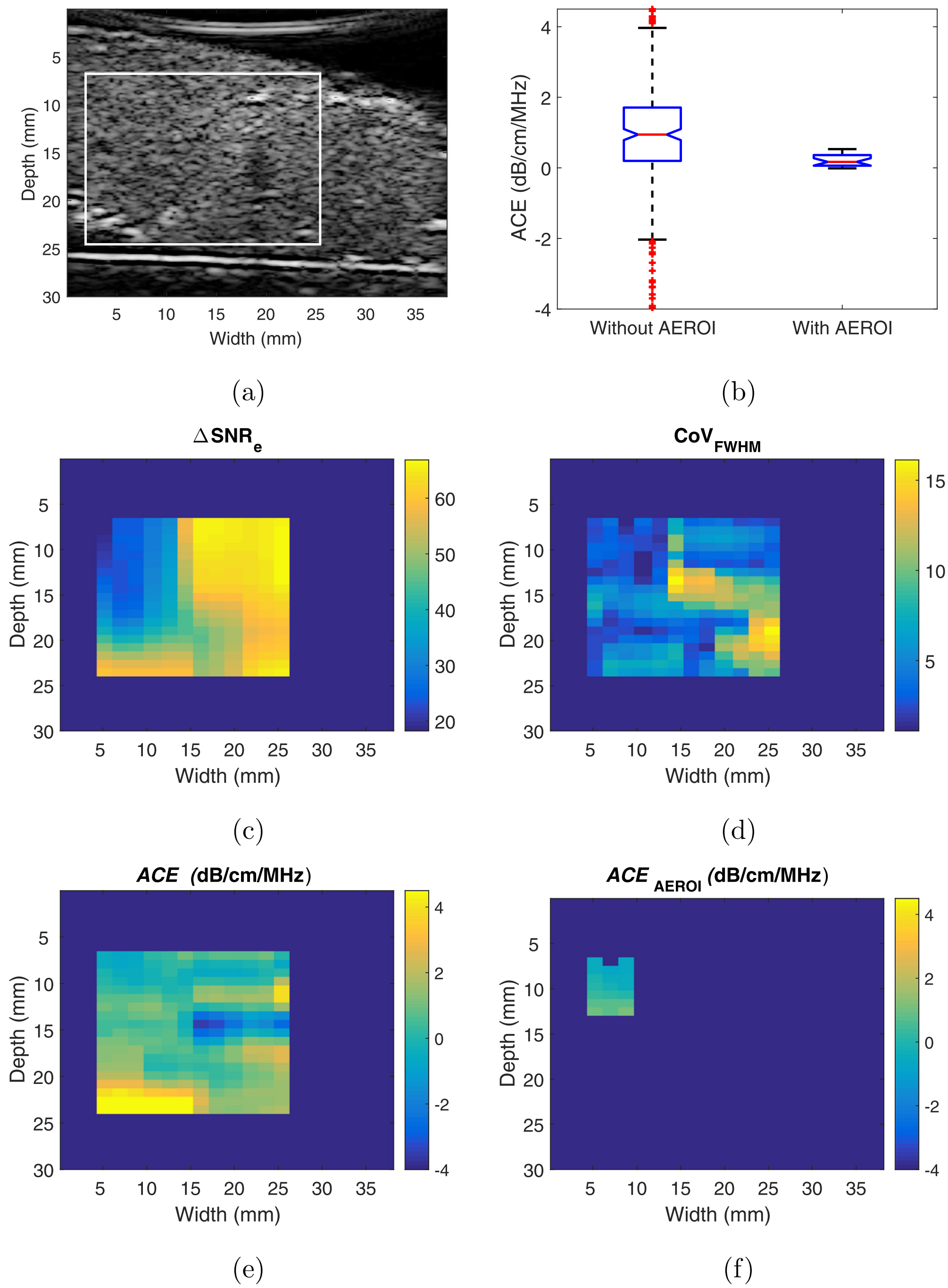

Fig. 4. Effect of AEROI selection method on attenuation coefficient estimate error for a typical *ex vivo* placenta sample. (a) B-Mode image with ROI defining the maximum rectangular area containing placental tissue; (b) Box-and-whisker representation of the attenuation coefficient estimates before and after applying the AEROI selection method; (c) ΔSNR_e map for the selected ROI; (d) CoV_{FWHM} map for the selected ROI; (e) Attenuation coefficient estimates in the ROI; (f) Attenuation coefficient estimates in the AEROI after applying the AEROI selection method. *ACE* = attenuation coefficient estimate; AEROI = attenuation estimation region of interest; CoV_{FWHM} = CoV of transmit pulse bandwidth; CoV = coefficient of variation; ΔSNR_e = envelope SNR deviation; SNR = signal-to-noise ratio.

bandwidth do not change in the process of attenuation. To our knowledge, our study is the first to explicitly describe the correlations of envelope SNR deviation and pulse bandwidth variation to the *ACE* error and estimate variance. We found that the outlying *ACE* contributing to the increased variance arises predominantly from the

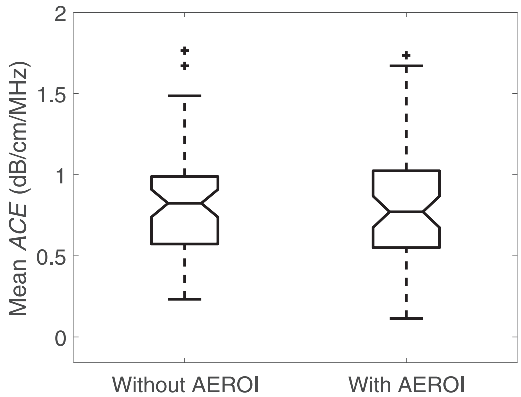

(a)

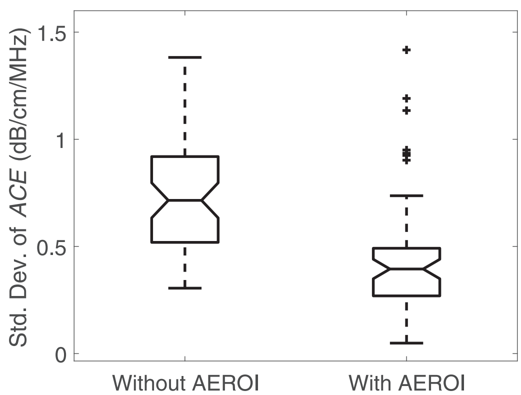

(b)

Fig. 5. Attenuation coefficient estimate for *ex vivo* placentas before and after applying AEROI selection method: (a) box and whisker representation of mean *ACE*; (b) box and whisker representation of intra-sample standard deviation of *ACE*. *ACE* = attenuation coefficient estimate; AEROI = attenuation estimation region of interest.

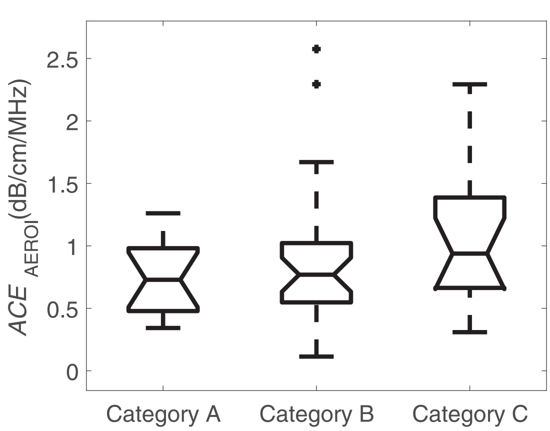

Fig. 6. Box and whisker representation of ACE_{AEROI} for three categories of *ex vivo* placenta data. *ACE* = attenuation coefficient estimate; AEROI = attenuation estimation region of interest.

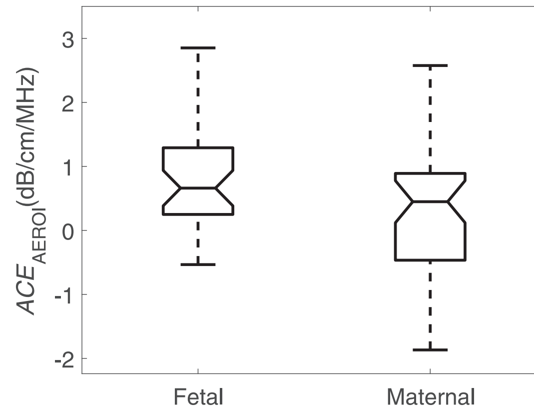

Fig. 7. Box and whisker representation of ACE_{AEROI} for region of interest near the fetal surface and near the maternal surface.

inhomogeneities in the sample. The outlying *ACE* also coincides with high envelope SNR deviation and pulse bandwidth variation. Therefore, imposing the AEROI selection criteria based on envelope SNR and pulse bandwidth essentially excludes most of the inhomogeneous regions. However, we acknowledge that we may lose clinically important information while discarding inhomogeneous regions. As the spectral difference and spectral shift methods will fail to measure *ACE* in the case of rapid change in the scatterer characteristics, improved methods could be devised for estimating *ACE* in the inhomogeneous regions.

We also reported the *ACE*s obtained from tissues near the fetal and maternal surfaces. We found that the *ACE* values at the fetal surface are slightly higher than those at the maternal surface, where the difference in median values is statistically significant. This could be a consequence of the relatively larger (stem) villi present on the fetal side. Finally, we analyzed the *ACE* values in relation to birth weight ($R^2 = 0.04$), placental weight ($R^2 = 0.04$), placental volume ($R^2 = 0.003$), placental density ($R^2 = 0.07$) and birth weight-to-placental weight ratio ($R^2 = 0.006$). We did not find any significant correlation between *ACE* and any of these parameters.

The RF data utilized for *ACE* computation in this study were acquired primarily for elastographic measurement of *ex vivo* placentas. This presents a unique advantage of the SWAVE system, which enables multi-parametric estimation yielding the elasticity and *ACE* maps with the same data. The simultaneous computation of *ACE* and elasticity with the same data reduces the scan time and obviates the requirement for registration. Previously, Fibroscan (Echosens, Paris, France), a vibration-controlled transient elastography device, provided similar capability for simultaneous measurement of liver elasticity and controlled attenuation parameter (Sasso et al. 2010). The main difference

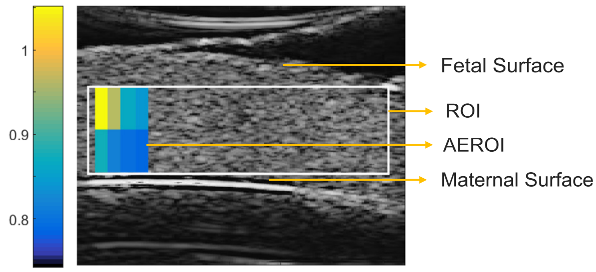

Fig. 8. An ACE_{AEROI} map as an overlay on the B-mode image of an *ex vivo* placenta. *ACE* = attenuation coefficient estimate; AEROI = attenuation estimation region of interest.

between the SWAVE system and Fibroscan is that SWAVE provides a 2-D elasticity map and a 2-D *ACE* map as an overlay on the B-mode ultrasound image, rather than a median estimate providing a single value. As an example, an *ACE* map has been presented as an overlay on the B-mode image of an *ex vivo* placenta in Figure 8.

The *ACE* could be a potential biomarker in assessing placental health. The validity of the utility of *ACE* in differentiating normal and pathologic placentas needs to be determined in future studies.

CONCLUSIONS

The placenta has received relatively little attention in the literature compared with other organs. This article describes the largest study to date to report *ACE* values based on the examination of 59 clinically normal placentas. This study establishes a robust and accurate *ACE* measurement method to measure *ex vivo ACE*s of human placentas. An AEROI selection method was proposed and validated on tissue-mimicking phantoms. The AEROI selection method was able to significantly reduce the intra-sample *ACE* variance. We report the *ACE* in *ex vivo* placenta to be 0.77 dB/cm/MHz, which is in agreement with the previous results. Future studies are required to compare the *ACE*s of normal and pathologic placentas.

Acknowledgments—This work was supported by the Natural Sciences and Engineering Research Council of Canada (NSERC) and the Canadian Institutes of Health Research (CIHR) (Grant CPG-146490).

REFERENCES

Abeysekera JM. Three dimensional ultrasound imaging. Ph.D. thesis. University of British Columbia; 2016.
Abeysekera JM, Ma M, Pesteie M, Terry J, Pugash D, Hutcheon JA, Mayer C, Lampe L, Salcudean S, Rohling R. SWAVE imaging of placental elasticity and viscosity: Proof of concept. Ultrasound Med Biol 2017;43:1112–1124.
Akaiwa A. Ultrasonic attenuation character estimated from backscattered radiofrequency signals in obstetrics and gynecology. Yonago Acta Med 1989;32:1–10.
Benson DM, Waldroup LD, Kurtz AB, Rose JL, Ritkin MD, Goldberg BB. Ultrasonic tissue characterization of fetal lung, liver, and placenta for the purpose of assessing fetal maturity. J Ultrasound Med 1983;2:489–494.
Bigelow TA, McFarlin BL, O'Brien WD, Jr., Oelze ML. In vivo ultrasonic attenuation slope estimates for detecting cervical ripening in rats: Preliminary results. J Acoust Soc Am 2008;123:1794–1800.
Caloone J, Huissoud C, Vincenot J, Kocot A, Dehay C, Chapelon JY, Rudigoz RC, Melodelima D. High-intensity focused ultrasound applied to the placenta using a toroidal transducer: A preliminary ex-vivo study. Ultrasound Obstet Gynecol 2015;45:313–319.
D'Astous FT, Foster FS. Frequency dependence of ultrasound attenuation and backscatter in breast tissue. Ultrasound Med Biol 1986;12:795–808.
Flax SW, Pelc NJ, Glover GH, Gutmann FD, Mclachlan M. Spectral characterization and attenuation measurements in ultrasound. Ultrason Imaging 1983;5:95–116.
Glüer CC. Quantitative ultrasound techniques for the assessment of osteoporosis: Expert agreement on current status. J Bone Miner Res 1997;12:1280–1288.
Grannum PA, Berkowitz RL, Hobbins JC. The ultrasonic changes in the maturing placenta and their relation to fetal pulmonic maturity. Am J Obstet Gynecol 1979;133:915–922.
Hyungsuk K, Varghese T. Attenuation estimation using spectral cross-correlation. IEEE Trans Ultrason Ferroelectr Freq Control 2007;54:510–519.
Kanayama Y, Kamiyama N, Maruyama K, Sumino Y. Real-time ultrasound attenuation imaging of diffuse fatty liver disease. Ultrasound Med Biol 2013;39:692–705.
Khong TY, Mooney EE, Ariel I, Balmus NC, Boyd TK, Brundler MA, Derricott H, Evans MJ, Faye-Petersen OM, Gillan JE, Heazell AE, Heller DS, Jacques SM, Keating S, Kelehan P, Maes A, McKay EM, Morgan TK, Nikkels PG, Parks WT, Redline RW, Scheimberg I, Schoots MH, Sebire NJ, Timmer A, Turowski G, Van Der Voorn JP, Van Lijnschoten I, Gordijn SJ. Sampling and definitions of placental lesions: Amsterdam placental workshop group consensus statement. Arch Pathol Lab Med 2016;140: 698–713.
Kuc R, Schwartz M, Micsky LV. Parametric estimation of the acoustic attenuation coefficient slope for soft tissue. Proc IEEE Int Ultrason Symp 1976;44–47.
Labyed Y, Bigelow TA. A theoretical comparison of attenuation measurement techniques from backscattered ultrasound echoes. J Acoust Soc Am 2011;129:2316–2324.
Liu W, Zagzebski JA, Liu W. Trade-offs in data acquisition and processing parameters for backscatter and scatterer size estimations. IEEE Trans Ultrason Ferroelectr Freq Control 2010;57:340–352.
Lu ZF, Zagzebski JA, Lee FT. Ultrasound backscatter and attenuation in human liver with diffuse disease. Ultrasound Med Biol 1999;25:1047–1054.
McFarlin BL, Bigelow TA, Laybed Y, O'Brien WD, Oelze ML, Abramowicz JS. Ultrasonic attenuation estimation of the pregnant cervix: A preliminary report. Ultrasound Obstet Gynecol 2010;36:218–225.
Nam K, Rosado-Mendez IM, Rubert NC, Madsen EL, Zagzebski JA, Hall TJ. Ultrasound attenuation measurements using a reference phantom with sound speed mismatch. Ultrason Imaging 2011;33:251–263.
Nam K, Zagzebski JA, Hall TJ. Quantitative assessment of in vivo breast masses using ultrasound attenuation and backscatter. Ultrason Imaging 2013;35:146–161.
O'Donnell M, Mimbs JW, Miller JG. Relationship between collagen and ultrasonic backscatter in myocardial tissue. J Acoust Soc Am 1981;69:580–588.
Oelze ML, O'Brien WD. Frequency-dependent attenuation-compensation functions for ultrasonic signals backscattered from random media. J Acoust Soc Am 2002;111:2308–2319.
Omari E, Lee H, Varghese T. Theoretical and phantom based investigation of the impact of sound speed and backscatter variations on attenuation slope estimation. Ultrasonics 2011;51:758–767.
Omari EA, Varghese T, Madsen EL, Frank G. Evaluation of the impact of backscatter intensity variations on ultrasound attenuation estimation. Med Phys 2013;40 082904.

Rosado-Mendez IM, Nam K, Hall TJ, Zagzebski JA. Task-oriented comparison of power spectral density estimation methods for quantifying acoustic attenuation in diagnostic ultrasound using a reference phantom method. Ultrason Imaging 2013;35:214–234.

Rosado-Mendez I, Drehfal L, Zagzebski J, Hall T. Analysis of coherent and diffuse scattering using a reference phantom. IEEE Trans Ultrason Ferroelectr Freq Control 2016;63:1306–1320.

Rubert N, Varghese T. Scatterer number density considerations in reference phantom-based attenuation estimation. Ultrasound Med Biol 2014;40:1680–1696.

Sasso M, Beaugrand M, de Ledinghen V, Douvin C, Marcellin P, Poupon R, Sandrin L, Miette V. Controlled attenuation parameter (CAP): A novel VCTE guided ultrasonic attenuation measurement for the evaluation of hepatic steatosis: Preliminary study and validation in a cohort of patients with chronic liver disease from various causes. Ultrasound Med Biol 2010;36:1825–1835.

Shankar PM, Molthen R, Narayanan VM, Reid JM, Genis V, Forsberg F, Piccoli CW, Lindenmayer AE, Goldberg BB. Studies on the use of non-Rayleigh statistics for ultrasonic tissue characterization. Ultrasound Med Biol 1996;22:873–882.

Shi H, Varghese T, Mitchell CC, McCormick M, Dempsey RJ, Kliewer MA. In vivo attenuation and equivalent scatterer size parameters for atherosclerotic carotid plaque: Preliminary results. Ultrasonics 2009;49:779–785.

Wear KA. Characterization of trabecular bone using the backscattered spectral centroid shift. IEEE Trans. Ultrason Ferroelectr Freq Control 2003;50:402–407.

Welch PD. The use of fast fourier transform for the estimation of power spectra: A method based on time avraging over short, modified periodograms. IEEE Trans Audio Electroacoust 1967;15:70–73.

Yao LX, Zagzebski JA, Madsen EL. Backscatter coefficient measurements using a reference phantom to extract depth-dependent instrumentation factors. Ultrason Imaging 1990;12:58–70.

Yassin L, Bigelow TA, McFarlin BL. Estimate of the attenuation coefficient using a clinical array transducer for the detection of cervical ripening in human pregnancy. Ultrasonics 2011;51:34–39.